Macromolecules

ARTICLE

pubs.acs.org/Macromolecules

Growth Pathway and Precursor States in Single Lamellar Crystallization: MD Simulations

Chuanfu Luo* and Jens-Uwe Sommer

Leibniz Institute of Polymer Research Dresden, Hohe Str 6, 01069 Dresden, Germany

ABSTRACT: Large-scale and long-time molecular dynamics (MD) simulations are carried out to study the growth pathway of a single polymer crystal from an entangled dense melt via self-seeding. Using the concept of lifetime of individual stems, we can identify two stages of crystallization. The stem length increases linearly with its lifetime at the first stage (precursor stage) while it increases logarithmically at the following stage (thickening stage). Folds are created at the precursor stage, and refolding events are statistically irrelevant. This analysis concurs with the direct observation of a precursor zone around the growth front as defined by orientational order of segments. Precursor states can be identified as bundles of short stems which do not cover the growth front densely.

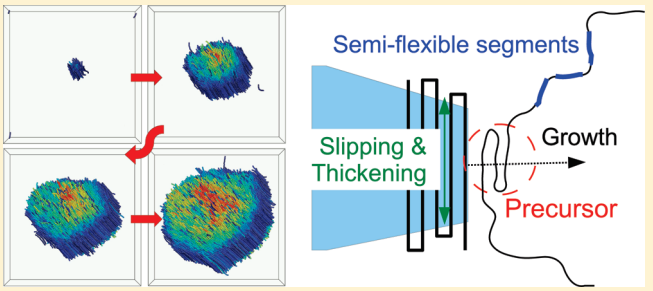

I. INTRODUCTION

The understanding of polymer crystallization is a long-standing problem of polymer science.[1−3] The classical models proposed by Lauritzen/Hoffman (LH)[4−6] and Sadler/Gilmer (SG)[7,8] have several points in common: First, they are based on a one-stage process explaining polymer crystallization as a single-step kinetic process involving either a nucleation (LH) or an entropic barrier (SG). Second, the chains rest in their nonequilibrium structure once crystallized. With the beginning of the 1990s, new experimental observations of very early stages of polymer crystallization have triggered a reconsideration of these classic theories and challenge them in their basic assumptions.[9−16]

The difficulty of developing a consistent theory lies in the fact that semicrystalline polymers are far from thermodynamic equilibrium (highly dependent on the thermal history) and that the kinetics of individual polymer chains are rather difficult to be observed in experiments. In order to obtain such information, computer simulations can monitor the conformations and dynamics of individual polymer chains directly at monomer scale. Monte Carlo (MC) and molecular dynamics (MD) simulations have been applied to study polymer crystallization processes at different scales of coarse graining.[3,17−27] Recently, by very large-scale MD simulations, Gee et al. were able to identify Cahn−Hilliard-type density fluctuations as well as indications for the emergence of small smectic regions within the crystallization process.[28,29] However, the formation and growth of individual crystalline lamellae could not be observed in these simulations.

A common problem of all computer simulations carried out so far are the extremely high cooling rates and high supercoolings which are necessary due to limited computational resources. Thus, homogeneous nucleation prevails which leads to many small and rather unstable crystallites which are prone of rapid reorganization.[28,30] This is in contrast to the experimental situation where single lamellar growth is dominating, and it is this process which is addressed by most theoretical models.

In this work we apply a self-seeding (or self-nucleation) protocol[31,32] to obtain well-defined single-lamellar growth in melts of long chains. This allows us to study the growth pathway and folding kinetics of individual chains during lamellar growth. The rest of the work is organized as follows: The simulation model and details of the simulation procedure are presented in section II. In section III, the concept of orientational−temporal persistence is introduced, and the growth pathway, folding kinetics, and evidence of precursor stage during the lamellar growth are discussed. Our conclusions are presented in section VI.

II. SIMULATION MODEL AND SELF-SEEDING PROCEDURE

The coarse-grained model of poly(vinyl alcohol) (CG-PVA) proposed by Meyer and Müller-Plathe is applied[33,34] with our patch code for LAMMPS.[35−37] Within the CG-PVA model, reduced units are used. The length unit is 0.52 nm, and the bond length is b_0 = 0.5 = 0.26 nm. The mass (m) and Boltzmann constant (k_B) are reduced to 1. The reduced temperature of T = 1 corresponds to 550 K. The time unit is estimated as 3.5 ps. In fact, it is difficult to accurately map the unit to real time. The value of 3.5 ps is estimated from equivalent Rouse relaxation time. The time step of MD integration is 0.01 (∼35 fs). Periodic boundary condition and NPT ensemble (at 1 atm) are applied by a Brendsen barostat (with the damp time of 1000 MD steps) and a Nos-Hoover thermostat (the damp time of 100 MD steps).

Received: October 19, 2010
Revised: January 24, 2011
Published: February 21, 2011

dx.doi.org/10.1021/ma102380m | *Macromolecules* 2011, 44, 1523–1529

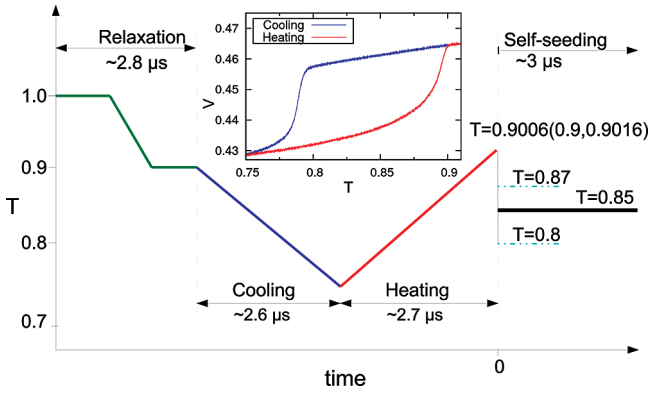

Figure 1. Temperature protocol for self-seeding. The initial conformation is taken from self-avoiding random walks and then relaxed during 8×10^7 MD steps at $T = 1.0-0.9$. Continuous cooling of the quiescent melt is performed from $T = 0.9$ (495 K) to 0.75 (385 K) by 7.5×10^7 MD steps (~2.6 μs), followed by heating the system to $T = 0.9$ or slightly above (0.9006 or 0.9016) at the same rate. Finally, the system is quenched to lower constant temperatures, $T = 0.87$, 0.85, or 0.8. The inset is the evolution of volume per monomer (v) with temperature for the cooling/heating cycle.

The whole system consists of 10^6 monomers (1000 chains of 1000 monomers each), and the box size is about 77.5 (~39 nm).

In Figure 1, we display the temperature protocol of our simulations. The inset shows the volume per monomer (v) versus temperature (T) during the cooling−reheating cycle indicating the crystallization/melting hysteresis for polymers. The crystalline state at $T = 0.75$ contains many small crystallized domains, which are the result of homogeneous nucleation since the cooling rate in computer simulations is much faster than that in common experiments. This is a general and crucial problem of simulations of polymer crystallization. To overcome this limitation and to obtain well-controlled single-lamellar growth, we apply a self-seeding procedure which allows us to reduce the supercooling and to avoid homogeneous nucleation for a long period.

The self-seeding procedure is implemented as follows: When we raise the temperature to about $T = 0.9$, most of the crystallized domains are molten, while a part of the most stable domain is still surviving due to a reorganization process which has been studied in detail in our previous work.[30] Now, we select this survival part as the initial seed and let it grow again by quenching the system to a lower constant temperature. This process is called self-seeding or self-nucleation. We will focus on the self-seeding process in the following and show that how it can provide a large single lamellar crystal. We tried several different pairs of initial and final temperatures as sketched in the right part of Figure 1. A large single crystal is obtained only from $T = 0.9006$ quenched to 0.85. All seeds are unstable at $T = 0.87$, and the seed from 0.9016 is unstable at all quenched temperatures. The seeds (from $T = 0.9006$ and 0.9 to 0.8 and from $T = 0.9$ to 0.85) are stable and grow, but other small domains appear again rapidly because of the deep quenching. In the following, we will discuss the growth of the single lamella as obtained from the quench $T = 0.9006$ to 0.85 in detail.

III. RESULTS AND DISCUSSION

A. A Measure for Crystallization far from Equilibrium: Orientational−Temporal Persistence. To analyze the simulation data, we need a molecular definition of crystallization which can be applied far from equilibrium and to detect rapidly changing structures. The concept of static order parameters like crystallinity or orientational (tensor) order become volatile (such as the concept of a crystalline stem) because the state of order is rapidly changing. Alternative measures of order based on the diffusion coefficient[38,39] are also not suited to discriminate between disordered and precursor states. This is exactly the problem in experiments, where a direct detection of a precursor state for polymer crystallization turns out be extremely difficult using standard methods such as scattering or calorimetry. In the following we propose an entirely new concept for crystallinity which combines persistence in time and orientational order. Therefore, it can be applied to strongly fluctuating states where traditional concepts of order parameters would fail.

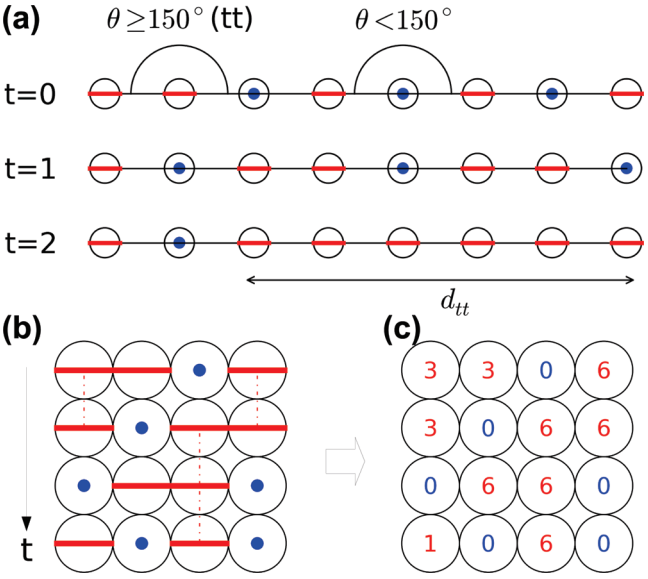

Figure 2. Definition of a measure for orientational−temporal persistence: (a) Sketch of the definition of stem length (d_{tt}) by successive trans−trans (tt) monomers. (b, c) Sketch of definition of domains in index−time space and their size. The monomers in successive tt states are collected having strong orientational correlations in index space and thus in real space (thick red lines). Two monomers at successive times are collected if they are both in tt states and are thus persistent in time (dashed red lines). The domain is defined as the cluster of connected monomers in the index−time space with size (S_d) denoting the number of monomers within the domain, as show in (c).

To define the new order parameter, we first define the length of a stem (d_{tt}) by the length of successive trans−trans (tt) monomers along the chain at a given moment of time. Please note that, we will use the reduced length unit (which corresponds to 0.52 nm) but not the number of monomers in the follow discussions. A monomer is in trans−trans state if the total bond angle satisfies $\theta \geq 150°$ (see Figure 2a). (The value of 150 is taken from the distribution of angles shown in Figure 4b, at which the population is almost zero and not sensitive to the values of 150 ± 5°.) To define a measure of crystallinity under nonequilibrium conditions, we also consider the persistence of the tt-states during time evolution of the system. Our idea is sketched in Figure 2: Instead of using the length of the stems only, which might be present only via a very short time scale, we define domains which consist of connected tt-states in the combined (monomer) index−time space. Thus, the index−time domain size, S_d, is related to the correlation in space and time. It is

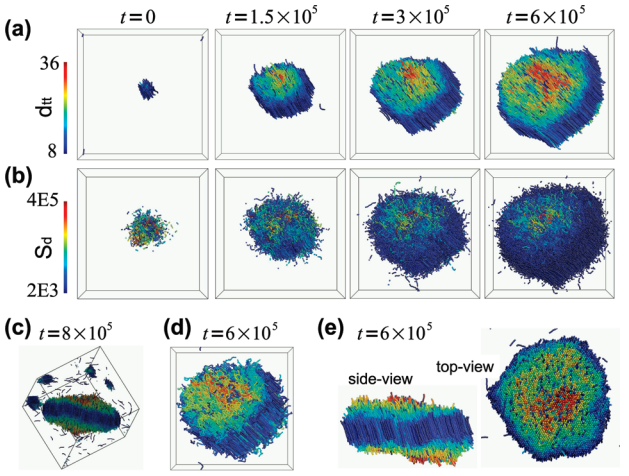

Figure 3. Snapshots of single lamellar growth at $T = 0.85$, self-seeded from $T = 0.9006$. (a) Monomers are colored by stem length d_{tt}. (b) Monomers are colored by the domain size in index−time space (S_d). This figure shows the space distribution of monomers with higher stiffness (larger S_d value). (c) Snapshot at $t = 8 \times 10^5$, monomers are colored by d_{tt}. (d) Snapshot at $t = 6 \times 10^5$ with surface region (the monomers share the same color value of the collected stems), monomers are colored by d_{tt}. (e) Side view and top view of the single lamella at $t = 6 \times 10^5$.

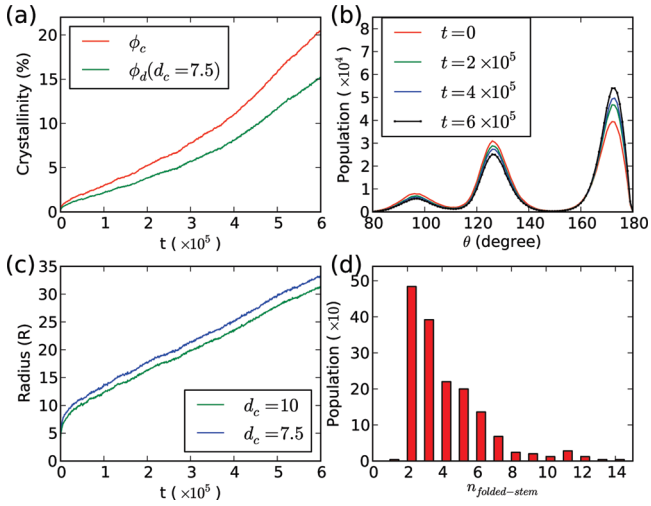

Figure 4. (a) Growth of whole crystallinity with time. (b) Distributions of angles at different time. (c) Growth of radius of the single lamellar crystal with time. (d) Distributions of number of the folded stems (formed at almost the same time) attached to the crystal.

also related to the thermal stability of a certain segment of polymer chains. A higher value of S_d indicates that a certain segment is more persistent in space and time. In general, the parameter S_d has the dimension of length × time. In our case, we can reduce it to the number of collected monomers in index-time space (see Figure 2b) using the same time interval $\Delta t = 10^3$(~3500 ps) throughout this work.

We mention that the orientational−temporal persistence can be viewed as a new kind of unnormalized order parameter, which is defined in index and time space while usual order parameters are defined in Cartesian space. The advantage of using orientational−temporal persistence is that it can give the order distribution along chain index with a proper time average, which is important to detect order on finite time scales for the study of folding kinetics. The order parameter can be defined for single stems because of the finite time domain used. We note that this is not easily possible for static order parameter because here stems can disappear by sliding and reorganization processes and reappear at other (nearby) parts of the system. We note that for characterization of the order of the stable crystalline part we use static order parameters as well and we prove their failure for the discrimination of precursor states.

B. Growth of the Single Lamella. Using the self-seeding procedure described in section II, we were able to grow a single crystalline lamella under conditions available in computer simulations. The snapshots of the growth of the single lamella are shown in Figure 3, colored by the stem length (d_{tt}) and domain size (S_d) in index−time space, respectively. From the Figure 3a,b, we can see that the initial seed grows to a single large lamellar crystal from $t = 0$ to $t = 6 \times 10^5$ (Figure 3b also shows some information of precursor state which we will discuss later). After $t = 6 \times 10^5$, some small crystals appear and grow around the single crystal (see the snapshot in Figure 3c at $t = 8 \times 10^5$). This may be caused by the limited size of the simulation box which hinders further growth of the lamella and triggers the nucleation of small crystals. Moreover, the temperature of $T = 0.85$ is still under deep quenching, and after sufficient relaxation time, chains start to crystallize via homogeneous nucleation. Actually, the occurrence of further homogeneous nuclei (not close to the main crystal) is due to the thermal history as well as the limited box size; a single crystal without further homogeneous may be obtained by carefully optimized thermal path. Therefore, we restrict our analysis of lamellar growth up to $t = 6 \times 10^5$. Here, about 20% of the monomer units are contained in the crystalline phase, and the single crystal is large enough (already close to the box size) to analyze its properties and growth kinetics.

In Figure 3d,e, we show the snapshot with surface region, the side view, and top view of the single lamella at $t = 6 \times 10^5$. It is obvious that the lamellar surface is rough and the stems at the edge are shorter than those in the middle (caused by lamellar thickening if we consider the time evolution). Here, we mention that the term "rough" is on the molecular length scale (of nanometers), which is much smaller than the length scale in usual experiments (of micrometers). Furthermore, reorganization processes[30,40] on larger length scales can lead to smooth growth fronts at larger time scales.Thus, the roughness of the growth front in our simulations does not necessarily conflict with the observation of smooth interface under microscopies. (For a detailed discussion we refer to the classical literature; see ref 41.) Further, we observe a tilt angle between the stem direction and the normal of lamellar plan.

The roughness of lamellar surface at the nanometer range and thickening of the lamella are not consistent with the original LH theory, and also different from the SG theory, indicating that the kinetics at molecular scale differs from that assumed in classic models for growth of polymer crystals under the conditions used in our simulations.

In Figure 4a, we show the growth of accumulative crystallinity with time estimated by two methods: The accumulative crystallinity can be defined either by the average volume fraction of the crystalline state (ϕ_c) or by number fraction of monomers in stems (ϕ_d). The first observable (ϕ_c) is calculated from the volume per monomer (v) and can be written as

$$\phi_c = (v_m - v)/(v - v_c) \quad (1)$$

dx.doi.org/10.1021/ma102380m |Macromolecules 2011, 44, 1523–1529

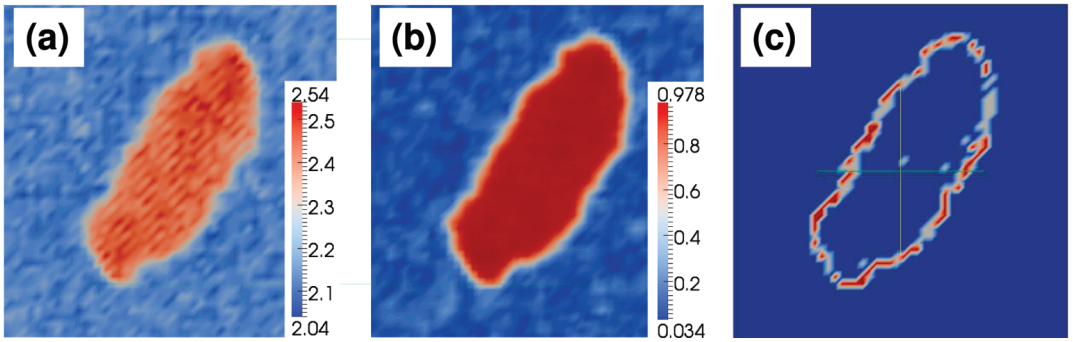

Figure 5. Comparison of local density and local tensor order (section view). (a) Local number density (D). (b) Local tensor order parameter (S). (c) Surface layer (intersection of $D < 2.4$ and $S > 0.5$), which is discontinuous. The simulation box is cut into a grid of $50 \times 50 \times 50$ cells, and D and S are calculated for each cell. The green horizontal lines are used to guide eyes.

Here $\nu_m = 0.461$ and $\nu_c = 0.415$ are the volumes per monomer in the melt and in the crystal state at $T = 0.85$, respectively. The second observable (ϕ_d) is calculated by the number fraction of monomers forming stems, $\phi_d = M_c/M$, where M_c is the number of monomers forming stems (crystalline state) and M is the total number of monomers in the system. Here, we use a cutoff for the stem length, $d_c = 7.5$, and only the stems with $d_{tt} > 7.5$ are considered (15 successive tt-states). The two methods are different in the way how to treat the surface region (with higher density than melt, see the white part around the crystal in Figure 5a). In general, ϕ_c is always overestimated for including the surface and ϕ_d is underestimated for excluding the surface. We can see that the two methods show good consistence if we consider a factor about 1.3 (ϕ_c/ϕ_d), which indicates that the thickness of surface is almost constant and the simple stem length d_{tt} can be used.[30] We mention that the difference between ϕ_c and ϕ_d is not due to the small crystalline clusters because there is no stable cluster far from the growth front during the time window of $t < 6 \times 10^5$ and the growth trends of ϕ_c and ϕ_d are the same.

We found that the increase of crystallinity is not linear with time. At the first glance, it seems that our results conflict with the observations of constant growth rate in most experiments. We will show that it is the result of thickening of lamella at the early stage (our single crystal can be considered as the early stage when compared to experiments), and the constant lateral growth rate can be observed if we measure the radius of the lamella rather than the accumulative crystallinity.

We show the growth of radius, R, of the single crystal in Figure 4c. The radius is calculated by

$$R = \sqrt{n_{stem}/\sigma\pi} \tag{2}$$

Here n_{stem} is the number of stems, and σ is the number density of stems in the 2D plane vertical to the stem direction. The stems in crystalline state are hexagonally densely packed, and the value of $1/\sigma = 0.83$ can be estimated by the position of the first Bragg peak ($q_{peak} = 7.41$) in the calculated structure factor at $T = 0.85$ ($1/\sigma = (3^{1/2}/2)r_0^2$, $r_0 = 4\pi/(3^{1/2}q_{peak})$. Unlike the accumulative crystallinity, the rate of lateral growth is constant and thus consistent with most experimental observations. The different cutoff values of stem lengths (d_c) only affect the thin layer at the growth front and do not change the observed linear growth of the radius.

Generally, the crystalline part has higher density or larger orientational order. To analyze the spatial distribution of order, the simulation box is divided into a grid of $50 \times 50 \times 50$ cells. For each cell we calculated the local number density (D) and local tensor order parameter (S) at $t = 6 \times 10^5$. The results are compared in the Figure 5. The local tensor order parameter (S) reflects the orientational order of bonds in a given cell, which is defined as

$$S = \sqrt{\frac{3}{2}\mathrm{Tr}Q^2}, \quad Q_{\alpha\beta} = \left\langle \hat{b}_\alpha \hat{b}_\beta - \frac{1}{3}\delta_{\alpha\beta} \right\rangle \tag{3}$$

Here, Tr denotes trace operator, Q is a 3×3 orientational tensor with components of $Q_{\alpha\beta}$, $\hat{b}$ is the normalized bond vector in 3D space, and $\alpha, \beta = 1, 2, 3$ are the spatial components (x, y, and z). The symbol $\langle \cdots \rangle$ denotes the statistical average over all bonds in a given cell (also averaged over a time interval of 100 in our case, 10 configurations are used).

We find a thin layer of about 0.8 nm (about the size of one cell) of rather large tensor order ($S = 0.5-0.7$) near the growth front, while in the same region of space the density is low (almost the same as in the melt). This layer is explicitly displayed in Figure 5c. Obviously, near the growth front some segments of polymer chains have already be partially aligned but are not densely packed. The chains near the growth front can be considered as the very early stage of a crystal. In the following we will analyze the growth process in more details at molecular scale.

C. Folding Kinetics and Precursor States. To obtain an intuitive picture of the crystallization pathway, snapshots of a single chain at different times are shown in Figure 6a. Typically, the chain first forms a number of short folded stems, and then these stems grow. We mention that these stems appear at the lamellar edge (the growth front, not shown in the figure). We emphasize that the intrachain effect is as important as interchain effect in our simulations, and this process can be considered as intrachain nucleation because the chain in our simulation is very long,[21] although the intrachain nucleation is originally proposed in the study of primary nucleation.In particular, we observe: (1) The stem length is increasing with time. (2) The stems are folded instantaneously, not one by one. This is obviously different from classical crystallization theory. (3) Before folding, the segments are forming looplike structures first. This may be considered as the beginning of precursor state. (4) We find that chains are not fully crystallized during the time window of our simulations; i.e., parts of the chain are still in melt state, which is important for the slipping of polymer chains as discussed further below.

In Figure 6b,c, we analyze the index−time space of the same chain shown in Figure 6a by means of angle (θ) and domain size

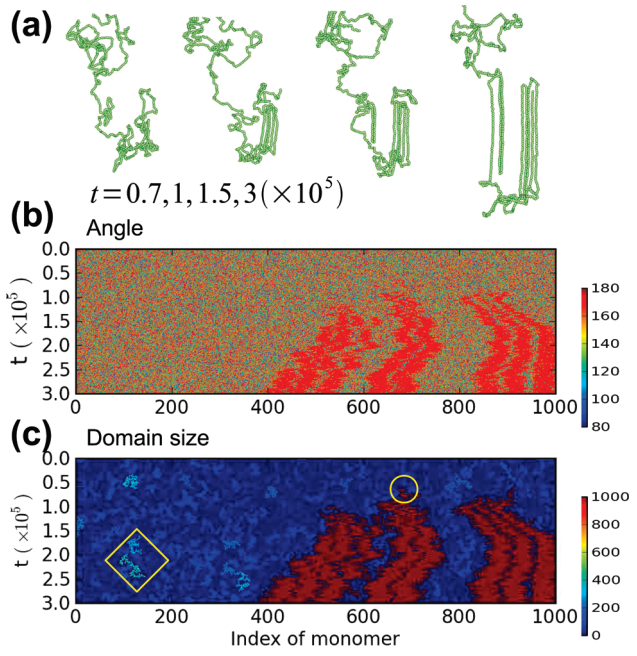

Figure 6. Folding pathway of a single chain. (a) Snapshots at different time. (b) Colored by angle (θ) in index−time space. The red belts correspond to stems. The increase of stem length and slipping along the stem direction (the slope of red belts) is obvious. (c) Colored by domain size (S_d) in index−time space. There are many small domains (semiflexible segments) in the blue area (melt state), indicating that those segments have some kind of persistence. The yellow circle and diamond indicate the precursor stage of a stem and a semiflexible segment, respectively.

(S_d). From the two figures, the slipping motion (the slope of the red belts) is obvious, and the increase of stem length is also clearly visible. We also see that stems are folded instantaneously and then grow in length. The number of folded stems ($n_{\text{folded-stem}}$, which is defined as the number of stems of a bundle formed at almost the same time) is almost constant during our simulation. We analyzed all the chains (1000) and found that the reorganization of folding happened only three times. Thus we can calculate the distribution of the number of folds ($n_{\text{folded-stem}} - 1$) from the distribution of $n_{\text{folded-stem}}$ displayed in Figure 4d. Apparently, most chains form single-folded (hairpin) and double-folded structures.

In Figure 6c, we also observe many small domains (semiflexible segments, one example is indicated by a yellow diamond) at the melt state. These small domains fluctuate with time and possess a significant value of S_d (200−400). Still, these segments have some kind of stiffness and can be distinguished from the melt state. (The average value of S_d at melt state is mainly depended on temperature.) These semiflexible segments are formed by part of chains in which some sequences are stiff while others are soft. The stiff sequences can survive for a short time in free melt state (see the small domains in the left of Figure 6c) but can survive longer near the growth front and can be changed into crystalline stems when nucleated. Please note that the stem is a stiff part of a minimum length of 7.5 (15 monomers) in our discussions, which is different from the semiflexible segment.

The precursor states of stems in index−time space can also be found in Figure 6c (the loose networks/domains at the birth of stems; one example is indicated by a yellow circle). The precursor states of stems are of the very early stages of stems formed from

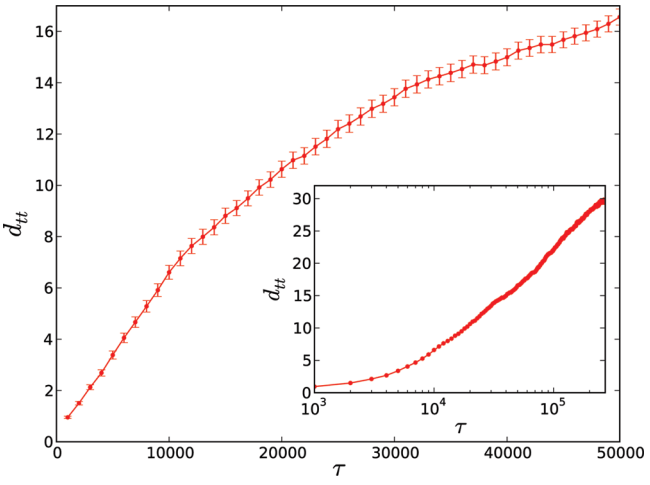

Figure 7. Growth of stem length with its lifetime. Linear growth can be found at $\tau < 12\,000$. The inset is plotted by semilog axes, and the logarithmic growth can be found at $\tau \gtrsim 1.2 \times 10^4$.

semiflexible segments. In Figure 3b, we show the snapshots with monomers colored by the domain size, S_d. By comparing it to Figure 3a, we can see that many monomers (of precursor stage whose value of domain size is large enough) appear around the crystallized part, especially near the growth front. These monomers are stiff parts of chains (yet not stems) and will change into stems later.

The trigger of crystallization (stems from semiflexible segments) may be the conformational confinement (like on surfaces or near impurities) which reduces the conformational entropy of nearby chains. From the snapshot at $t = 0$ of Figure 3b, we can also see that the ratio of monomers at precursor state is large, which leads to the fast growth rate at the beginning (see Figure 4a,c). It means that stiff chains during the heating process are not fully relaxed (as our initial seed at $t = 0$ is taken from the remain part of a crystalline domain). These incompletely molten chains have semistiff segments and may be the reason for the fast growth rate obtained in self-seeding (self-nucleation) experiments.

The folding kinetics observed in our simulations can be viewed as a kind of molecular nucleation. Wunderlich and Mehta observed the rejection of lower molecular weights from growing crystal surfaces, which indicates a molecular nucleation.[42] In our simulations, we did not found such kind of length selected effect because the chains have the same length. But from the growth kinetics (chains are folded first), we suggest that it is a molecular nucleation process.

D. Growth History of Individual Stems. The analysis in index−time space allows us to trace back the birth time (t_0) of each stem and thus define the lifetime ($\tau = t - t_0$) of individual stems. Using this information, we can analyze the rate of increase in stem length according to the lifetime. Because lateral growth of the lamella is a linear function of time, from the relation between stem length and lifetime the relation between the stem length and the distance from the growth front can be obtained as well. In Figure 7 we display the average stem length (of all chains) as a function of lifetime. Two stages in the growth of stem length can identified.

First, for lifetimes $\tau < 12\,000$ (~45 ns), a linear growth regime is observed. During this stage, the precursor semiflexible segments near the growth front try to crystallize. It is reasonable to assume that precursor (semiflexible) segments have a higher free

dx.doi.org/10.1021/ma102380m |*Macromolecules* 2011, 44, 1523–1529

energy as compared to crystalline segments but also higher entropy than the stiff stems. Thus, the enthalpy of stiff stems has to be much lower than that of precursor segments, which means that the density of the precursor segments is much lower than that for crystallized stems and should be close to the density of melt state (we have seen this in Figure 5). In this linear regime of stem length growth we have $d_{tt} = c\tau$, where c is a constant (related to the temperature and polymer structure) which reflects how often a monomer attempts to crystallize before it is incorporated into the crystal. We note that the stem length at the end of precursor stage is about 8 (4.16 nm, about 1/4 of the final stem length), which may be related to the empirical correction factor in the critical lamellar thickness formula.[43]

Second, for $\tau \geq 12\,000$, stem length growth becomes logarithmic (see inset of Figure.7). We can assume that this is a slipping-and-thickening process according to the analysis of folding pathways (see Figure 6b,c). By assuming an energy barrier which is proportional to the stem length (d_{tt}), the growth rate can be written as $\dot{d}_{tt} = c' \exp[(-\Delta E/T)d_{tt}]$, which leads to

$$d_{tt} = d_0 + \frac{T}{\Delta E}[\ln(\tau/\tau_0)] \quad (4)$$

where ΔE is the energy barrier for slipping and thickening per monomer, c' is a constant, τ_0 is the precursor time (about 12 000 in our case), and d_0 is the stem length at the end of precursor ($\tau = \tau_0$). The energy barrier, ΔE, may be closely related to polymer species, and it is smaller if the monomer is smoother ($\Delta E \cong 0.12$ in our case). The two different schemes in growth of stem length support the picture of precursor states and a two-stage crystallization pathway via prestiffened polymer chains.

The logarithmic growth does not cease within the simulation time (see Figure 7). As a consequence, stems in the center of the lamella are still growing, and the shape of the lamella is not flat. Taking into account the linear relation for radial growth (see Figure 4c), the thickness profile of the lamalla is logarithmic, too. This, however, is hard to discriminate from a constant thickness in experiments if one also takes into account some roughness of the crystal surface (see the snapshot in Figure 3e). We note that lamellar thickening has been clearly observed in particular in thin polymer films.[44]

The above analysis allows us to identify the thin surface layer we found in Figure 5 with the precursor stage. The radial thickness of precursor stage (d) can be estimated by $d = g\tau_0$ if we assume it does not change during the steady growth of crystal (the growth rate is equal to the change rate from precursor stage to stems); here the growth rate of radius ($g = 4 \times 10^{-5}$) can be calculated from the slope in Figure 4c. The result is $d = 0.48$ (0.25 nm), which is only about 1/3 of the estimated thickness from Figure 5 (about 1 grid, ≃0.8 nm) and even smaller than the size of one stem (≃0.51 nm).

However, the surface layer at the growth front in Figure 5c is rough, and the chains are first folded at the precursor stage (most are single-folded or double-folded) and form small folding clusters. Thus, the precursor layer around the growth front is formed of individual clusters (with higher local orientational order parameter) (see Figures 3e and 5c). The degree of coverage of the growth front by precursors should be the ratio of thickness estimated from radial growth rate over that from tensor order, which is about 1/3. Therefore, we can conclude that the discontinuous surface layer at the growth front in Figure 5c is the precursor layer, which is formed of many discrete folding clusters. The sizes of small folding clusters are about 0.8 nm, which corresponds to the size of a bundle of 2−4 stems.

We mention that the existence of precursor state at the growth front is physically reasonable, but it is difficult to "be observed" just by "looking at" the snapshots. Many previous MD simulations did not find precursor states near the growth front,[28,29,45,46] or the evidence is not so clear.[47] The precursor layer is very thin, and the segments are changing very fast. The usual concept of instantaneous "stem" is difficult to distinguish the precursor state from melt or crystal. The combination of tensor order and orientational−temporal persistence described in our article is essential. Moreover, large single-crystal growth via self-seeding removes the interactions between small crystalline domains (formed by homogeneous nucleation in most MD simulations), which makes the analyze easier and more reliable.

VI. CONCLUSIONS

Using large MD simulations of a coarse-grained PVA model, we simulated the growth pathway of a single lamellar polymer crystal obtained by a self-seeding protocol. Linear lateral growth, lamellar thickening, and slipping of monomers along chain direction are directly observed in our simulations. We have introduced a measure of orientational−temporal persistence to characterize the state of monomer sequences out of equilibrium. This analysis allows us to define a birth time for each stem, and accordingly, folding kinetics of individual chains is analyzed as a function of their lifetime. Two stages can be identified for the growth of stem length with lifetime: The stem length increases linearly with lifetime at the precursor stage while it increases logarithmically at the thickening stage.

The classical LH or SG models are not consistent with our results which correspond to a time scale of about ≲45 ns . We can identify a precursor state as an early stage of a stable stem from semiflexible segments. The semiflexible segments are possessing orientational−temporal persistence and are ready to crystallize (if temperature is low enough) and can be thus considered as unstable short stems. The semiflexible segments become oriented at the precursor stage near the growth front (possibly because of the effect of geometric restrictions). Semiflexible segments are first folded at the precursor stage, and the stem thickness is developed later. Folds (mostly single or double folding) are rarely changed during the following thickening stage. Over the time window of our simulations we recorded only about 0.3% of refolding events during the lifetime of a crystalline stem. However, the reorganization of folding may be still important for the further increase of stem length at longer time scales. The precursor layer around the growth front is discontinuous and formed of discrete folding clusters (with higher local orientational order parameter) containing bundles of 2−4 stems. The radial thickness of precursor layer is about 0.8 nm. Our simulation results show the evidence of at least two stages in polymer crystallization and indicate that folding and thickness selection may be different kinetic processes. We note that the time and space window in our simulation is still much shorter and smaller than that in experiments, and our simulations compare with the early stages of a crystal growth in experiments.

AUTHOR INFORMATION

Corresponding Author
*E-mail: luo@ipfdd.de.

■ ACKNOWLEDGMENT

The authors thank Deutsche Forschungsgemeinschaft (DFG) (SO 277/6-1) for financial support and Zentrum für Informationsdienste und Hochleistungsrechnen (ZIH) of Technische Universität Dresden for computing time. We also thank Hendrik Meyer and Günter Reiter for helpful discussions.

■ REFERENCES

(1) Strobl, G. *The Physics of Polymers*, 3rd ed.; Springer: Berlin, 2007.
(2) Sommer, J.-U., Reiter, G., Eds. *Polymer Crystallization: Observations, Concepts and Interpretations*; Lecture Notes in Physics Vol. 606; Springer: Berlin, 2003.
(3) Muthukumar, M. *Adv. Polym. Sci.* **2005**, *191*, 241.
(4) Hoffman, J. D. *J. Chem. Phys.* **1958**, *29*, 1192.
(5) Lauritzen, J. I.; Hoffman, J. D. *J. Appl. Phys.* **1973**, *44*, 4340.
(6) Hoffmann, J. D.; Davis, G. T.; Lauritzen, J. I. *The Rate of Crystallization of Linear Polymers with Chain Folding*; Plenum Press: New York, 1976; Vol. 3, pp 497−614, treatise in solid state chemistry ed.
(7) Sadler, D. M.; Gilmer, G. H. *Phys. Rev. Lett.* **1986**, *56*, 2708.
(8) Sadler, D. M. *Nature* **1987**, *326*, 174.
(9) Strobl, G. *Prog. Polym. Sci.* **2006**, *31*, 398.
(10) Strobl, G. *Rev. Mod. Phys.* **2009**, *81*, 1287.
(11) Imai, M.; Kaji, K.; Kanaya, T. *Macromolecules* **1994**, *27*, 7103.
(12) Imai, M.; Kaji, K.; Kanaya, T.; Sakai, Y. *Phys. Rev. B* **1995**, *52*, 12696.
(13) Olmsted, P. D.; Poon, W. C. K.; McLeish, T. C. B.; Terrill, N. J.; Ryan, A. J. *Phys. Rev. Lett.* **1998**, *81*, 373.
(14) Soccio, M.; Nogales, A.; Lotti, N.; Munari, A.; Ezquerra, T. A. *Phys. Rev. Lett.* **2007**, *98*, 037801.
(15) Sirota, E. B. *Macromolecules* **2007**, *40*, 1043.
(16) Panine, P.; Cola, E. D.; Sztucki, M.; Marayanan, T. *Polymer* **2008**, *49*, 676.
(17) Doye, J. P. K.; Frenkel, D. *Phys. Rev. Lett.* **1998**, *81*, 2160.
(18) Doye, J. P. K.; Frenkel, D. *J. Chem. Phys.* **1998**, *109*, 10033.
(19) Chen, C.-M.; Higgs, P. *J. Chem. Phys.* **1998**, *108*, 4305.
(20) Hu, W. *J. Chem. Phys.* **2001**, *115*, 4295.
(21) Hu, W.; Frenkel, D.; Mathot, V. B. F. *Macromolecules* **2003**, *36*, 8178.
(22) Sommer, J.-U.; Reiter, G. *J. Chem. Phys.* **2000**, *112*, 4384.
(23) Sommer, J.-U.; Reiter, G. *Europhys. Lett.* **2001**, *56*, 755.
(24) Reiter, G.; Sommer, J.-U. *Phys. Rev. Lett.* **1998**, *80*, 3771.
(25) Fujiwara, S.; Sato, T. *Phys. Rev. Lett.* **1998**, *80*, 991.
(26) Fujiwara, S.; Sato, T. *J. Chem. Phys.* **1999**, *110*, 9757.
(27) Welch, P.; Muthukumar, M. *Phys. Rev. Lett.* **2001**, *87*, 218302.
(28) Gee, R. H.; Lacevic, N. M.; Fried, L. E. *Nature Mater.* **2006**, *5*, 39.
(29) Lacevic, N. M.; Fried, L. E.; Gee, R. H. *J. Chem. Phys.* **2008**, *128*, 014903.
(30) Luo, C.; Sommer, J.-U. *Phys. Rev. Lett.* **2009**, *102*, 147801.
(31) Mamun, A.; Umemoto, S.; Okui, N.; Ishiharar, N. *Macromolecules* **2007**, *40*, 6296.
(32) Xu, J.-J.; Ma, Y.; Hu, W.; Rehahn, M.; Reiter, G. *Nature Mater.* **2009**, *8*, 348.
(33) Meyer, H.; Müller-Plathe, F. *J. Chem. Phys.* **2001**, *115*, 7807.
(34) Meyer, H.; Müller-Plathe, F. *Macromolecules* **2002**, *35*, 1241.
(35) Plimpton, S. *J. Comput. Phys.* **1995**, *117*, 1.
(36) Luo, C.; Sommer, J.-U. *Comput. Phys. Commun.* **2009**, *180*, 1382.
(37) Offical site is http://lammps.sandia.gov.
(38) Rapaport, D. *The Art of Molecular Dynamics Simulation*, 2nd ed.; Combridge University Press: New York, 1995.
(39) Koga, K.; Gao, G.; Tanaka, H.; Zeng, X. *Nature* **2001**, *412*, 802.
(40) Reiter, G.; Castelein, G.; Sommer, J.-U.; Röttele, A.; Thurn-Albrecht, T. *Phys. Rev. Lett.* **2001**, *87*, 226101.
(41) Armitstead, K.; Goldbeck-Wood, G. *Adv. Polym. Sci.* **1992**, *100*, 219.
(42) Wunderlich, B.; Mehta, A. *J. Polym. Sci., Polym. Phys. Ed.* **1974**, *12*, 255.
(43) Lan, Y.-K.; Su, A.-C. *Macromolecules* **2010**, *43*, 7908.
(44) Reiter, G.; Castelein, G.; Sommer, J.-U. *Phys. Rev. Lett.* **2001**, *86*, 5918.
(45) Yamamoto, T. *Polymer* **2004**, *45*, 1357.
(46) Yamamoto, T. *Adv. Polym. Sci.* **2005**, *191*, 37.
(47) Yamamoto, T. *J. Chem. Phys.* **2008**, *129*, 184903.